Bulgarian Chemical Communications, Volume 58, Special Issue A (pp. 35-43) 2026 DOI: 10.34049/bcc.58.A.SN-07

Application of adsorption isotherms for Cd(II) uptake by vine rod-derived biochar: a comparative study

V. Georgieva *, S. Syuleyman, L. Gonsalvesh, S. Mileva, D. Asamova, S. Genieva

Department of Chemistry, Burgas State University "Prof. Dr. Assen Zlatarov", 1 Prof. Yakimov Str., 8010 Burgas, Bulgaria

Received: August 12, 2025; Revised: January 06, 2026

This study examines the thermodynamic aspects of Cd(II) ion adsorption from aqueous solutions onto biochar derived from vine rods (BC-VR). Linear two- and three-parameter isotherm models were applied to characterize the adsorption process. Key physicochemical parameters were determined, and the models that best fit the experimental data were identified. The optimal isotherm model was chosen based on the coefficient of determination (R^2) and statistical error analysis. Model validation confirmed that the selected isotherm equations provide a reliable description of the distribution of Cd(II) ions between the liquid and biochar phases under the tested conditions, contributing to a deeper understanding of the adsorption mechanism and its thermodynamic behavior.

Keywords: Cd(II) adsorption, Thermodynamics, Linear isotherm modelling, Error analysis

INTRODUCTION

Cadmium was discovered in 1817 by the German chemist *Friedrich Strohmeyer* during the analysis of zinc-carbonate ores isolated as a by-product [1]. The newly found element "cadmium" is named from the Latin word *Cadmia* and the Greek word *καδμεία*, which were used to describe the common zinc ore, calamine [2]. During the 19th and 20th centuries, researchers focused on the properties and applications of cadmium. Cadmium is considered a transition metal, and its chemical properties resemble those of zinc and mercury. Although cadmium is relatively rare in its elemental form, it is frequently found as an impurity in zinc, lead, and copper ores [3]. Its natural origin is associated with geological processes, volcanic activity, forest fires, and its inherent presence in various environmental components. The cadmium content in the Earth's mantle is approximately 0.1 mg/kg, and it occurs in minerals such as CdS (greenockite, hawleyite), CdSe (cadmoselite), and others, or as an impurity in zinc and lead ores [4,5]. Cadmium concentrations vary significantly depending on the type of rock in the Earth's crust, with higher concentrations in sedimentary rocks (0.01-2.6 mg/kg) compared to magmatic (0.07-0.25 mg/kg) and metamorphic rocks (0.11-1.0 mg/kg) [1]. During weathering and erosion of rocks and minerals, cadmium is gradually released into the soil and water, contributing to its presence in the environment. Volcanic activity is also a significant factor: volcanic eruptions can release cadmium-containing ash and gases into the atmosphere. Although the amount of cadmium released during volcanic activity is relatively small compared to other sources, it can still contribute to local soil and water contamination upon deposition. Forest fires also release cadmium, as organic substances from vegetation and soil are emitted into the atmosphere and land. While the immediate effect of forest fires on cadmium mobility may be limited, this process could pose future problems as the released cadmium may accumulate in ecosystems.

Natural sources of cadmium include not only rocks and minerals but also sediments, soils, air, and natural waters, where its concentrations vary considerably. In soils, cadmium content typically ranges from 0.1 to 1 mg/g, but certain regions and geographical areas have significantly higher levels. Certain regions in Europe, including Ireland, Poland, Goslar (Germany), and Southern Sardinia, have been identified as areas with elevated cadmium levels [6–8]. Although cadmium readily accumulates in the soil, its bioresistance causes it to be released slowly and inefficiently. Due to its high mobility in the environment, significant amounts of cadmium enter freshwater basins, where sedimentation occurs and cadmium is integrated into groundwater. Between 140 and 1,500 tons of cadmium into the atmosphere annually, with weathering of rocks playing a substantial role in its mobilization [9]. Approximately 50% of the cadmium is transferred into water bodies, with the remaining portion being released into the atmosphere through volcanic eruptions and forest fires.

* To whom all correspondence should be sent:
E-mail: *velyana_topalska@btu.bg*

There are also anthropogenic sources of cadmium, such as mining processes, metal refining, battery production, and the use of paints and pigments, which release significant amounts of cadmium into the environment [1]. Global annual cadmium production has steadily increased, from 18,100 tons in 1994 to a peak of 25,000 tons in 2017, with a slight decrease to 23,000 tons in 2023 [10]. Canada is the leading producer of cadmium, with major consumers including Japan, Mexico, the USA, and Peru [11, 12]. Zinc, lead, and copper mining releases significant amounts of cadmium, which affects soil and water quality. In China, cadmium concentrations in wastewater from areas where lead-zinc ores are mined or processed have been recorded at 2-4 times the permissible limits for drinking water (5 μg/dm^3 [11]) [3]. The burning of fossil fuels in power plants and industrial facilities is another anthropogenic source of cadmium through dust and gas emissions, which can travel long distances and contaminate soils and waters.

Cadmium possesses unique toxicological properties, making it a serious environmental issue. It is highly persistent in the environment, can accumulate in soils, sediments, and organisms, and can bioaccumulate through the food chain. Cadmium does not play a biological role in organisms, which is why it causes severe toxic effects. Its impact on the body includes damage to the cardiovascular, urinary, gastrointestinal, neurological, and respiratory systems. This heavy metal directly affects cellular division, potentially causing cell death. It has been found to induce genetic mutations and chromosomal abnormalities by inhibiting DNA replication. Its toxicity is linked to the suppression of cellular respiration and the activity of key antioxidant enzymes [2, 13]. Humans are protected from chronic exposure to low cadmium concentrations by the presence of metallothioneins – a group of small, widely distributed proteins rich in cysteine, which regulate zinc metabolism. Metallothioneins play a crucial role in protecting against ion toxicity from several heavy metals, DNA damage, and oxidative stress. The biological half-life of cadmium in the bloodstream is estimated to range from 75 to 128 days, reflecting its accumulation in organs rather than the rate of body clearance [2, 5]. According to the World Health Organization, the temporary acceptable weekly intake of this heavy metal is 2.5 μg/kg body weight [14], with concentrations above this limit considered hazardous to health.

To reduce Cd(II) pollution, it is essential to implement strict control measures on sources of contamination and proper waste management, including wastewater treatment. Given the widespread contamination with cadmium and its low recommended levels in drinking water, there is significant interest in developing effective methods for removing this metal from contaminated waters. Various technologies have been developed for treating industrial wastewater containing heavy metals, including adsorption, chemical precipitation, ion exchange, and membrane filtration. Among these, adsorption has become a proven and effective method for removing heavy metals from water and soil [15]. In the search for renewable energy sources, biomass has emerged as a promising source of chemical feedstocks. Biochar, a porous carbonaceous material obtained by pyrolyzing carbon-rich biomass in an oxygen-limited environment, is considered a promising, cost-effective, and efficient adsorbent for heavy metal removal from water. This is due to the presence of polar functional groups, such as carboxyl, hydroxyl, and amino groups, which facilitate the adsorption of heavy metals. Biochar from vine rods, a carbon-rich, porous material typically produced by thermally decomposing biomass in an oxygen-deprived environment, is regarded as a promising alternative adsorbent for various pollutants.

Accurate modeling of adsorption isotherms is crucial for the effective understanding and optimization of heavy metal removal processes. Although classical two-parameter models such as Langmuir and Freundlich provide valuable baseline information, three-parameter isotherm models offer greater flexibility and can more accurately capture the complexity of adsorption phenomena by accounting for additional physicochemical interactions. The present study investigates the applicability and performance of linear two and three-parameter isotherm models in describing the adsorption of Cd(II) ions onto biochar derived from vine rods. By conducting a comparative analysis, this study seeks to advance the understanding of the physicochemical properties of the examined adsorbent and elucidate the adsorption mechanism, ultimately supporting the design of more efficient biochar-based remediation approaches.

EXPERIMENTAL

Adsorbent preparation

Vine rods were sourced from the processing of *Vitis* plants in proximity to the town of Pomorie, Bulgaria. The initial treatment of this agro-waste material involved rinsing with distilled water, followed by air drying, grinding, and sieving through a 2 mm mesh to standardize particle size. The resulting material underwent slow pyrolysis in a

VEB Elektro Bad Frankenhausen LM 312.11 electric muffle furnace (Germany), conducted in a nitrogen atmosphere (99.9% purity). The temperature was increased gradually at a rate of 10 K/min to 773 K, with each 373 K increment maintained for 1 hour. After pyrolysis, the biochar was sieved, and the fraction with particle sizes ranging from 63 to 250 μm was selected for tests in the adsorption experiments.

Adsorbent characterization

The specific surface area of the obtained biochar was determined using the procedure described in the reference [16]. Surface functional groups of the tested biochar were identified in the range of 4000–400 cm^{-1} using a Nicolet iS 50 FTIR spectrometer (Thermo Scientific) to assess the possible interactions with the applied adsorbate.

Adsorbate

The stock solution containing 1000 mg/L of Cd(II) was prepared by dissolving 2.744 g of $Cd(NO_3)_2 \cdot 4H_2O$ (Merck) in ultrapure water. Working solutions of Cd(II) with concentrations ranging from 5 to 200 mg/L were subsequently prepared by serial dilution of the stock solution with ultrapure water.

Adsorption experiments

Adsorption experiments were conducted by varying the pH in the range of 2.5 to 8.5 for a contact time of 24 h, using a fixed adsorbent dose of 0.3 g, an initial concentration of 5 mg/L, and a constant temperature of 298 K. The desired pH values were adjusted by adding appropriate amounts of 0.1 M HCl or 0.1 M NaOH to the respective solutions. A volume of 100 mL of the test solution and 0.3 g of the adsorbent were placed in 200 mL iodine flasks and incubated in a Memmert WB22 (Germany) water bath equipped with a shaking system. The temperature was maintained with a precision of ±0.5°C.

Thermodynamic studies were carried out at the optimized pH value at three different temperatures (293, 298 and 303 K) and six initial concentrations ranging from 5 to 200 mg/L for 24 hours, using a fixed adsorbent dose of 0.3 g. Samples taken before and after the adsorption process were analyzed according to the standard BDS EN ISO 17294-2:2016 using an ICP-MS mass spectrometer, model iCAP Q (Thermo Scientific).

The percent removal of Cd(II) ions by BC-VR ($R_{Cd(II)}$, %) and the equilibrium adsorption capacity (Q_{eq}, mg/g), representing the amount of ions adsorbed per unit mass of adsorbent, were calculated using the following equations:

$$R_{Cd(II)},\% = \frac{C_o - C_{eq}}{C_o} \times 100 \quad (1)$$

$$Q_{eq} = \frac{C_0 - C_t}{m} \times V, \quad (2)$$

where C_o is the initial concentration of Cd(II) ions and C_{eq} - the concentration at equilibrium, mg/L, V is the solution volume, L, and m is the weight of the adsorbent, g.

Adsorption isotherms

Equilibrium adsorption data are typically interpreted using isotherm models, which provide a reliable means for understanding the underlying adsorption mechanisms, estimating the maximum adsorption capacity, and assessing the characteristics of the adsorbent. In this study, the adsorption behavior was examined by applying nine different isotherm models (Table 1).

The experimental results were processed using Microsoft Excel (Office 2019, USA), and the model parameters were obtained through linear regression analysis. Although the coefficient of determination (R^2) serves as the primary indicator for model fitting, it does not alone ensure model validity. Therefore, additional statistical criteria namely, the chi-square (χ^2) test and Marquardt's percentage standard deviation (*MPSD*) – were also employed, following the formulas provided in reference [19]. The Akaike Information Criterion (*AIC*) is a widely used metric for model evaluation and selection, combining goodness of fit and model complexity (number of parameters, p). It is calculated as follows [19]:

$$AIC = n \ln\left(\frac{SSE}{n}\right) + 2(p+1) + \frac{2(p+1)(p+2)}{n-p-2}, \quad (12)$$

where n is the number of experimental data, *SSE* – sum of the squares of errors [19, 26]. A lower *AIC* value indicates a better balance between data fit and simplicity. By penalizing excessive complexity, *AIC* helps prevent overfitting and supports the selection of models with good predictive performance.

Table 1. The applied isotherm models

Isotherm model	Linear form	Slope, Intercept	Eqs.	Ref.
Freundlich (Fr)	$\ln Q_{eq} = \ln K_F + \frac{1}{n_F} \ln C_{eq}$	Slope $1/n$, Int. $\ln K_F$	(3)	[17]
Langmuir (L)	$\frac{C_{eq}}{Q_{eq}} = \frac{1}{K_L Q_{max}} + \frac{1}{Q_{max}} C_{eq}$	Slope $1/Q_{max}$, Int. $1/K_L Q_{max}$	(4)	[18, 19]
Dubinin Radushkevich (D-R)	$\ln Q_{eq} = \ln Q_{DR} - K\varepsilon^2$, $RT \ln\left(1+\frac{1}{C_{eq}}\right) = \varepsilon$	Slope K_{DR}, Int. $\ln Q_{DR}$	(5)	[17, 20]
Temkin (Tem)	$Q_{eq} = B \ln A_T + B \ln C_{eq}$, $\frac{RT}{b_T} = B$	Slope B, Int. $B \ln A_T$	(6)	[18]
Scatchard (Sc)	$\frac{Q_{eq}}{C_{eq}} = K_{Sc}\left(\vartheta_{Sc}^0 - Q_{eq}\right)$	Slope K_{Sc}, Int. $K_{Sc}\vartheta_{Sc}^0$	(7)	[21]
Redlich-Peterson (R-P)	$\ln\left(K_{RP}\frac{C_{eq}}{Q_{eq}} - 1\right) = \ln \alpha_{RP} + \beta_{RP} \ln C_{eq}$	Slope β_{RP}, Int. $\ln \alpha_{RP}$	(8)	[22]
Toth (Th)	$\frac{C_{eq}}{Q_{eq}} = \frac{1}{(Q_{Th})^{Th} K_{Th}} + \frac{C_{eq}}{(Q_{Th})^{Th}}$	Slope $(Q_{Th})^{-Th}$, Int. $\left((Q_{Th})^{Th} K_{Th}\right)^{-1}$	(9)	[23]
Radke-Prausnitz (R-Pr)	$\frac{C_{eq}}{Q_{eq}} = \frac{1}{K_{RPr} k_{rpr}} + \frac{C_{eq}^P}{k_{rpr}}$	Slope $\left(k_{rpr}\right)^{-1}$, Int. $\left(K_{RPr} k_{rpr}\right)^{-1}$	(10)	[20]
Sips (S)	$\ln\left(\frac{Q_{eq}}{Q_m - Q_{eq}}\right) = \frac{1}{n} \ln C_{eq} + \ln\left(b_s\right)^{1/n}$	Slope $\frac{1}{n}$, Int. $\ln\left(b_s\right)^{1/n}$	(11)	[24, 25]

RESULTS AND DISCUSSION

To determine the specific surface area of the studied material, the procedure described in reference [16] was employed. The iodine adsorption number, which reflects the material's ability to adsorb iodine from solution, serves as an indirect measure of surface area and is commonly used to assess the porosity of activated carbons. In this context, the derived iodine number falls within the range of 360–435 mg/g, suggesting that the material predominantly possesses microporous characteristics. These values indicate that the sample has promising potential for applications in adsorption processes, particularly for the removal of small-sized contaminants.

The FTIR spectra of the sample before and after Cd(II) adsorption are shown in Figure 1 to facilitate the identification of functional groups involved in surface interactions during the adsorption process.

The FTIR spectra of the biochar derived from vine roots, recorded before and after Cd(II) adsorption, exhibit no notable changes in the positions or intensities of the main absorption bands, indicating preservation of the material's surface functional groups during the adsorption process.

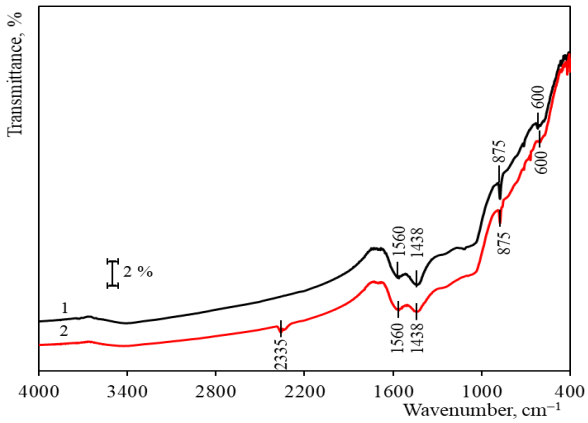

Fig. 1. FTIR spectra of BC-VR: 1 – before, 2 – after Cd(II) adsorption

The bands observed at 1560 cm^{-1} and 1428 cm^{-1} are assigned to the stretching vibrations of C=C bonds in alkenes and/or C–C bonds within aromatic ring structures. Out-of-plane deformation vibrations of =C–H groups are evidenced by the absorption bands at 875 cm^{-1} and 600 cm^{-1}, characteristic of aromatic moieties. A distinct band appearing at 2335 cm^{-1} in the spectrum of the sample after adsorption is attributed to the presence of physisorbed CO or CO_2 gases on the biochar surface [27], possibly due to exposure to atmospheric air or gas evolution

during adsorption. A comparative analysis of the FTIR spectra of biochar derived from vine rods and walnut shell biochar (WSBA, from our previous study [26]) reveals several common spectral features, suggesting structural similarities between the two materials. Both samples exhibit absorption bands around 1560 cm^{-1} and 1438–1428 cm^{-1}, which are attributed to the stretching vibrations of C=C bonds in aromatic rings, indicative of conjugated π-electron systems characteristic of partially carbonized structures. Additionally, both materials show bands near 875 cm^{-1}, associated with out-of-plane deformation vibrations of =C–H bonds in aromatic moieties. The vine rod biochar also exhibits a band at 600 cm^{-1}, which may correspond to additional deformation modes or arise from mineral components. Overall, the spectral profiles of both biochars suggest a predominantly aromatic structure with minimal contributions from oxygen-containing functional groups. The absence of significant spectral changes after Cd(II) adsorption onto vine rod biochar – analogous to the functional simplicity of WSBA – suggests that the adsorption process is likely governed by π–π interactions, surface area, and van der Waals forces, rather than by specific reactive surface functionalities.

The influence of temperature and solution pH on the removal efficiency of Cd(II) ions is presented in Fig. 2.

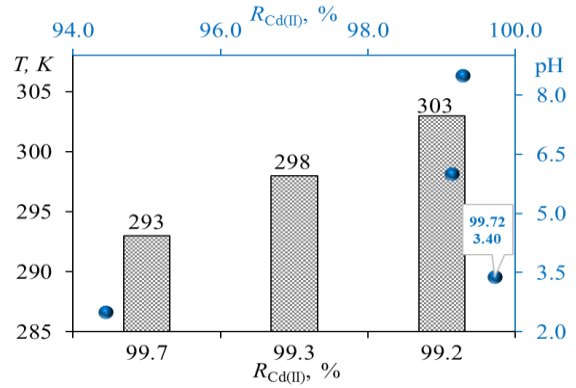

Fig. 2. pH and temperature effects onto adsorption process with BC-VR at initial Cd(II) concentration of 5 mg/L

The adsorption experiments conducted at 293, 298, and 303 K demonstrate that the removal efficiency remained consistently high, exceeding 99% under all investigated conditions. These results suggest that within the studied temperature range, thermal effects exert only a minor influence on the adsorption process, indicating that the interaction between Cd(II) ions and the bioadsorbent surface is not strongly temperature dependent. In contrast, the solution pH had a more pronounced effect on Cd(II) uptake. At highly acidic conditions (pH 2.5), the removal efficiency was significantly reduced (94.4%), which can be attributed to the competition between hydrogen ions and Cd(II) species for the active adsorption sites. As the pH increased to 3.40, the removal efficiency reached 99.72%, reflecting the reduced competition from protons and the enhanced availability of negatively charged functional groups on the adsorbent surface. Due to this maximum value of 99.72%, the pH of 3.4 was adopted as the optimal condition for the studied adsorption process. At pH values of 6.0 and 8.5, the removal efficiency remained very high and nearly constant (99.1–99.3%), suggesting that the bioadsorbent is highly effective over a broad pH range.

Overall, the results indicate that while the adsorption of Cd(II) onto BC-VR is only weakly affected by temperature, solution pH plays a decisive role in the process. The sharp increase in efficiency between pH 2.5 and 3.4 highlights the importance of electrostatic interactions and the ionization state of surface functional groups, whereas the stability of the efficiency at near-neutral and slightly alkaline conditions confirms the strong affinity of the adsorbent for Cd(II) ions.

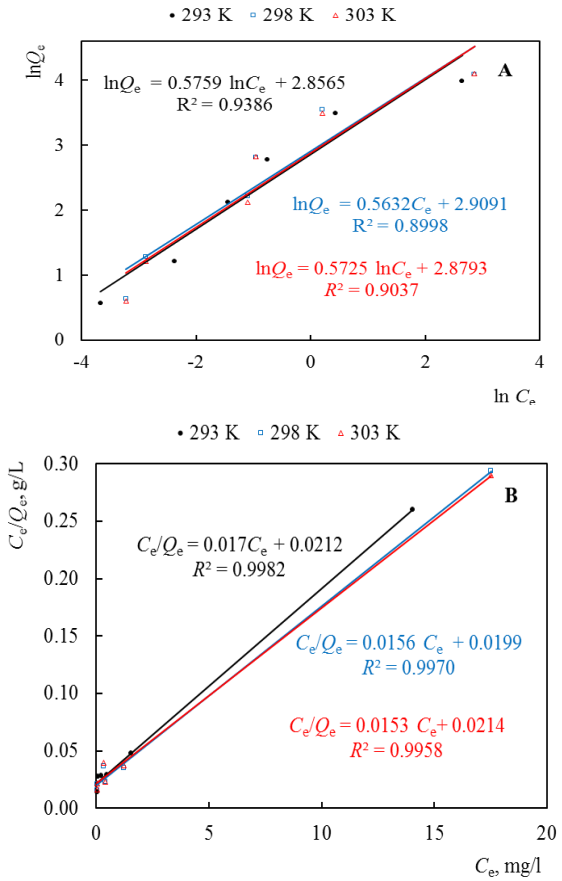

Fig. 3. Linear adsorption isotherms of *Freundlich* (A) and *Langmuir* (B) models for Cd(II) adsorption onto BC-VR at different temperatures

For the thermodynamic investigation of Cd(II) ion adsorption onto vine-rod biochar (BC-VR), experiments were performed within the concentration range of 5–200 mg/L under continuous maximum-speed shaking, at an adsorbent dose of 3 g/L, pH 3.4, and temperatures of 20, 25, and 30 °C. The obtained data were analyzed using all adsorption isotherm models described in the experimental section.

For a detailed characterization of the studied adsorption process, classical linearized isotherm models, such as those proposed by *Freundlich* and *Langmuir*, were employed. The graphical representations of these two isotherms are presented in Fig. 3.

The *Freundlich* equation fits at medium contaminant concentrations and energy heterogeneity at the adsorbent surface. It can be seen from Fig. 3A that there is no good linear correlation. The physicochemical parameters of the *Freundlich* isotherm are presented in Table 2. The *Langmuir* isotherm characterizes the process occurring on a homogeneous adsorbent surface with a uniform distribution of adsorption centers and no interaction between adsorbed molecules of the monolayer. By using the parameters from the *Langmuir* adsorption isotherm Q_{max} and K_L, the adsorption capacity and the suitability of the adsorbent under the tested conditions were evaluated by calculating the separation factor (R_L) [28].

Table 2. Error analysis and physicochemical parameters of linear isotherm models applied to Cd(II) adsorption onto vine-rod biochar at different temperatures

Isoth.	T, K	Parameters			R^2	χ^2	*MPSD*	*AIC*
		K_F ($L^{1/n}$ $mg^{1-1/n}$/g)	1/n					
Fr	293	17.40	1.74		0.939	15.4	37.2	47.3
	298	18.34	1.78		0.900	24.9	48.2	50.2
	303	17.80	1.75		0.904	23.6	46.9	79.7
L	T, K	K_L (L/mg)	Q_{max} (mg/g)	R_L	R^2	χ^2	*MPSD*	*AIC*
	293	0.80	58.77	6.50×10^{-3}	0.998	0.5	20.3	10.5
	298	0.78	63.98	6.54×10^{-3}	0.997	30.2	26.9	28.1
	303	0.72	65.29	6.25×10^{-3}	0.996	2.4	29.7	58.0
D-R	T, K	$K \times 10^8$ (mol^2/kJ^2)	Q_{DR} (mg/g)	E (kJ/mol)	R^2	χ^2	*MPSD*	*AIC*
	293	3.86	26.53	3.60	0.826	35.7	67.9	47.9
	298	4.42	32.45	3.36	0.883	2.4	77.3	48.0
	303	3.86	26.53	3.41	0.826	33.5	67.6	78.5
Tem	T, K	b_T (J/mol)	A_T (L/mg)		R^2	χ^2	*MPSD*	*AIC*
	293	273.5	20.83		0.939	5.11	215.7	36.3
	298	253.3	19.92		0.945	6.36	126.1	36.9
	303	255.5	18.93		0.943	11.53	169.2	67.2
Sc	T, K	K_{Sc} (L/mg)	ϑ_{Sc}^0 (mg/g)		R^2	χ^2	*MPSD*	*AIC*
	293	0.92	55.89		1.000	0.8	22.4	20.2
	298	0.80	65.57		0.737	31.4	28.4	27.9
	303	0.75	66.36		0.717	2.3	31.9	57.9
R-P	T, K	K_{RP} (L/g)	α_{RP} (L/mg)	β_{RP}	R^2	χ^2	*MPSD*	*AIC*
	293	94.63	3.81	0.595	0.935	6.73	9.8×10^2	71.2
	298	92.30	3.29	0.590	0.870	2.04	1.7×10^3	77.6
	303	2.0×10^6	1.1×10^5	0.428	0.840	23.56	5.4×10^1	1.2×10^3
Th	T, K	K_{Th} $(mg/L)^{Th}$	Q_{Th} (mg/g)	Th	R^2	χ^2	*MPSD*	*AIC*
	293	0.80	58.77	1.000	0.998	0.51	23.5	40.5
	298	0.79	64.97	0.996	0.997	0.30	31.5	57.9
	303	0.71	65.29	1.000	0.996	2.44	34.3	58.0

R-Pr	*T*, K	K_{RPr} (L/g)^P	k_{rpr} [(mg g^{-1}) /(mg L^{-1})]$^{1/P}$	*P*	R^2	χ^2	*MPSD*	*AIC*
	293	0.89	54.53	0.97	0.998	0.53	23.4	42.8
	298	0.68	71.51	1.04	0.997	0.51	31.3	57.0
	303	0.70	66.22	1.00	0.996	2.42	34.3	57.9
S	*T*, K	b_S (L/mg)	Q_m (mg/g)	1/*n*	R^2	$\chi 2$	*MPSD*	*AIC*
	293	0.72	60.67	0.992	0.992	1.09	26.0	46.8
	298	0.86	63.20	1.017	0.986	2.62	45.1	61.4
	303	0.77	64.67	1.002	0.984	2.34	42.4	57.7

In a similar manner, the experimental data were processed according to the two-parameter adsorption isotherms of *Dubinin–Radushkevich*, *Temkin*, and *Scatchard*, and the physicochemical parameters obtained for each isotherm are presented in Table 2.

The *Dubinin–Radushkevich* model supported physical adsorption based on the mean adsorption energy (*E*), which values are 3.36–3.60 kJ/mol (Table 2). Although the correlation coefficients are lower (R^2 = 0.826–0.883), the D–R model provides useful insights into the adsorption mechanism. The moderate variation of Q_{DR} with temperature (26.5–32.5 mg/g) is consistent with the observed temperature dependence. The *Temkin* constants revealed relatively high adsorption energy at the lowest temperature (b_T = 273.5 J/mol at 293 K), which decreases slightly with increasing temperature. This trend suggests stronger initial binding at low temperature, followed by a stabilization of adsorption sites at elevated temperatures. Although R^2 values (0.939–0.945) are acceptable, the large *MPSD* values (126–216) indicate a less precise description compared to the *Langmuir* model. The *Scatchard* model produced an excellent fit at 293 K (R^2 = 1.000), but the correlation decreased sharply at higher temperatures (R^2 = 0.717–0.737). This implies that the *Scatchard* equation may describe the adsorption process well under specific conditions (low temperature), but it is less reliable across the full temperature range. When a satisfactory agreement is obtained between the experimental data and the calculated values derived from the *Langmuir* isotherm equation, it is recommended to also apply alternative three-parameter isotherm models. These include the *Redlich–Peterson*, *Toth*, *Radke–Prausnitz*, and *Sips* isotherms. The application of such models provides higher accuracy in the determination of thermodynamic constants, which is particularly important for achieving a deeper understanding of the adsorption processes. For the analysis of the linear relationships characteristic of the respective isotherms, the Solver add-in of Microsoft Excel was employed to obtain maximum values of the coefficient of determination (R^2). At 293 K, the R–P model showed reasonable fitting (R^2 = 0.935) with β ≈ 0.6, reflecting intermediate behavior between *Langmuir* and *Freundlich* models. However, at higher temperatures, both the correlation and physical relevance of the constants deteriorated (e.g., extremely large values at 303 K), suggesting limited applicability of this model under the studied conditions. The *Toth* model yielded excellent agreement with experimental data (R^2 = 0.996–0.998). The values of the heterogeneity factor (Th ≈ 1) indicate that the surface behaves nearly homogeneously, consistent with the *Langmuir* assumption. The increasing Q_{Th} values with temperature confirm the enhanced adsorption capacity at higher temperatures. The three-parameter model R-Pr also showed very high correlation (R^2 = 0.996–0.998), with parameter *P* values close to unity, further supporting monolayer adsorption on a homogeneous surface. The results closely resemble those of the *Langmuir* and *Toth* models, reinforcing their suitability. The *Sips* model produced good correlations (R^2 = 0.984–0.992) with heterogeneity parameter 1/*n* close to unity, again suggesting that the adsorption system approaches *Langmuir*-type behavior. The maximum adsorption capacity (Q_m) increases slightly with temperature, in line with the other models.

Overall, the adsorption of Cd(II) onto BC-VR is best described by the *Langmuir* and *Sips* models, which exhibited the highest correlations (R^2 > 0.99), the lowest error values, and the most favorable *AIC* scores. Ultimately, the *Langmuir* isotherm emerges as the most appropriate model, as it is simpler (requiring fewer parameters than the *Sips* model) while consistently providing excellent results at all investigated temperatures. These findings confirm that the process follows monolayer adsorption on a relatively homogeneous surface with enhanced capacity at higher temperatures. To place the present results in context, the thermodynamic constants of Cd(II) adsorption obtained in this study were compared with literature data for other adsorbents (Table 3).

Table 3. Comparison of thermodynamic constants during adsorption of Cd(II) ions on different adsorbents

Adsorbents	Conditions	Q_{max}, mg/g	K_L, L/mg	Ref.
Pistachio hull waste	pH 5.5 (23±2°C)	14.90	0.0300	[29]
	pH 6.5 (23±2°C)	20.30	0.0600	
Biochars derived from grape vine shoots GVS-600	pH > 3	286.40	9.0590	[30]
Walnut shell	pH 6.0 (25°C)	7.29	0.0174	[31]
Oak bark biochar	pH 5 (25°C)	0.37	0.0377	[32]
Pine bark char		0.34	0.0002	
Oak bark biochar		5.40	0.0055	
Vine rod-derived biochar -Iran	pH 6.0 (40°C)	45.50	-	[33]
Phosphate modified grape branch biochar 0.2 PB	pH > 3 (25°C)	14.02	0.3320	[34]
Vine rod-derived biochar BC-VR	pH 3.4 (25°C)	64.27	0.8289	Present study

Table 3 summarizes the thermodynamic constants for various adsorbents, enabling comparison of the maximum adsorption capacity (Q_{max}) for Cd(II) removal from aqueous solutions. The data show that adsorption performance strongly depends on both the adsorbent type and experimental conditions. Among the reported materials, vine-rod biochar GVS-600 exhibits the highest adsorption capacity (Q_{max} = 286.4 mg/g), followed by the present study's biochar (BC-VR, Q_{max} = 64.3 mg/g) and vine-rod biochar from Iran (Q_{max} = 45.5 mg/g). In contrast, lower capacities were obtained for pistachio shells, phosphate-modified vine-rod biochar, walnut shells, and various wood-derived biochars. The K_L values confirm the superior affinity of GVS-600, while the BC-VR examined in this work also demonstrates competitive adsorption efficiency, highlighting its potential as a cost-effective material for Cd(II) removal from water.

CONCLUSIONS

Vine-rod biochar (BC-VR) proved to be a highly efficient and favorable adsorbent for Cd(II) removal from aqueous solutions. The process follows the *Langmuir* isotherm, confirming monolayer adsorption on a relatively homogeneous surface, with capacity increasing at higher temperatures. The predominantly aromatic structure with limited oxygen functionalities suggests that adsorption is governed mainly by π–π interactions, surface area, and van der Waals forces. Under optimized conditions (pH 3.4, dose 3 g/L), BC-VR demonstrates competitive adsorption capacity, highlighting its potential for practical water treatment applications.

REFERENCES

1. A. Dhanda, Ritambhara, S. Lamba, R. Prakash, in: *Cadmium Toxic. Water*, A. K. Jha, N. Kumar (eds.), 2024, p. 3.
2. M. Peana, A. Pelucelli, C. T. Chasapis, S. P. Perlepes, V. Bekiari, S. Medici, M. A. Zoroddu, *Biomolecules*, **13**, 1 (2023).
3. B. Du, J. Zhou, B. Lu, C. Zhang, D. Li, J. Zhou, S. Jiao, K. Zhao, H. Zhang, *Sci. Total Environ.*, **720**, 137585 (2020).
4. F. Pinot, S. E. Kreps, M. Bachelet, P. Hainaut, M. Bakonyi, B. S. Polla, *Rev. Environ. Health*, **15**, 299 (2000).
5. R. A. Bernhoft, *Sci. World J.*, 394652 (2013).
6. M. J. Canty, A. Scanlon, D. M. Collins, G. McGrath, T. A. Clegg, E. Lane, M. K. Sheridan, S. J. More, *Sci. Total Environ.*, **485–486**, 223 (2014).
7. E. A. Lane, M. J. Canty, S. J. More, *Res. Vet. Sci.*, **101**, 132 (2015).
8. J. Pan, J. A. Plant, N. Voulvoulis, C. J. Oates, C. Ihlenfeld, *Environ. Geochem. Health,* **32**, 1 (2010).
9. Council of Ministers, Cadmium Review 2003.
10. Y. Bin Yu, J. W. Lee, A. H. Jo, Y. J. Choi, C. Y. Choi, J. C. Kang, J. H. Kim, *Toxics*, **12**, 1 (2024).
11. G. Fatima, A. M. Raza, N. Hadi, N. Nigam, A. A. Mahdi, *Indian J. Clin. Biochem.*, **34**, 371 (2019).
12. Y. B. Gelaw, H. Dagne, B. Adane, G. Yirdaw, M. Moges, Z. Aneley, L. Kumlachew, A. Aschale, Y. A. Deml, E. Tegegne, T. A. Birhan, *Heliyon*, **10**, e40389 (2024).
13. K. Jomova, S. Y. Alomar, E. Nepovimova, K. Kuca, M. Valko, Heavy Metals : Toxicity and Human Health Effects , Springer, Berlin Heidelberg, 2025.
14. A. Cantoral, S. Collado-López, L. Betanzos-Robledo, H. Lamadrid-Figueroa, B. A. García-Martínez, C. Ríos, A. Díaz-Ruiz, R. M. Mariscal-Moreno, M. M. Téllez-Rojo, *Foods*, **13**, 3649 (2024).
15. R. Hamzenejad, E. Sepehr, A. Samadi, M. H. R. Sadaghiani, H. Khodaverdiloo, *J. Environ. Stud.*, **43**, 401 (2017).
16. a U. Itodo, F. W. Abdulrahman, L. G. Hassan, S. a Maigandi, H. U. Itodo, *New York Sci. J.*, **3**, 25 (2010).
17. P. S. Vassileva, L. P. Ivanova, A. K. Detcheva, *Bulg. Chem. Commun.*, **54**, 21 (2022).
18. B. Hazar, D. Şakar, *Bulg. Chem. Commun.*, **56**, 215 (2024).
19. Y. Wang, C. Wang, X. Huang, Q. Zhang, T. Wang, X. Guo, *Chemosphere*, **349**, 140736 (2024).

20. S. Bbumba, *Adv. Image Video Process.*, **12**, (2024).
21. H. Saad, F. A. Nour El-Dien, N. E. A. El-Gamel, A. S. Abo Dena, *RSC Adv.*, **14**, 1316 (2024).
22. K. H. Chu, M. A. Hashim, Y. T. da C. Santos, J. Debord, M. Harel, J. C. Bollinger, *Chem. Eng. Sci.*, **285**, 119573 (2024).
23. M. G. Davis, K. Yan, J. G. Murphy, *Biogeosciences*, **21**, 5381 (2024).
24. A. M. Carvajal-Bernal, F. Gomez-Granados, L. Giraldo, J. C. Moreno-Pirajan, *Eur. J. Chem.*, **8,** 112 (2017).
25. S. Svilović, D. Rušić, R. Stipišić, N. Kuzmanić, *Bulg. Chem. Commun.*, **52**, 189 (2020).
26. V. G. Georgieva, L. Gonsalvesh, M. P. Tavlieva, *J. Mol. Liq.*, **312**, 112788 (2020).
27. B. Smith, Infrared Spectral Interpretation, CRC Press, February 6, 2018.
28. M. Prelac, I. Palčić, D. Cvitan, D. Anđelini, M. Repajić, J. Ćurko, T. K. Kovačević, S. Goreta Ban, Z. Užila, D. Ban, N. Major, *Materials (Basel).*, **16**, 4716 (2023).
29. M. Hamidpour, N. Hosseini, V. Mozafari, M. Heshmati Rafsanjani, *Rev. Int. Contam. Ambient.*, **34**, 307 (2018).
30. H. Li, D. Yao, Q. Feng, H. Zeng, J. Liang, Z. Zhou, Y. Tian, N. Zhou, X. Lu, *Desalin. Water Treat.*, **118**, 195 (2018).
31. R. Najam, S. M. A. Andrabi, *Desalin. Water Treat.*, **57**, 27363 (2016).
32. D. Mohan, C. U. Pittman, M. Bricka, F. Smith, B. Yancey, J. Mohammad, P. H. Steele, M. F. Alexandre-Franco, V. Gómez-Serrano, H. Gong, *J. Colloid Interface Sci.*, **310**, 57 (2007).
33. R. Hamzenejad, E. Sepehr, A. Samadi, M. H. Rasouli Sadaghiani, H. Khodaverdiloo, *J. Environ. Stud.*, **43**, 401 (2017).
34. Y. Han, Y. Yin, H. Zhang, S. Sun, Z. Huang, Y. Deng, L. Bao, *J. Geosci. Environ. Prot.*, **12**, 59 (2024).